Real-Time Radar Rainfall Estimation. Part II: Case Study

EMMANOUIL N. ANAGNOSTOU* AND WITOLD F. KRAJEWSKI

Iowa Institute of Hydraulic Research, University of Iowa, Iowa City, Iowa

(Manuscript received 7 August 1997, in final form 15 May 1998)

ABSTRACT

The performance of a real-time radar rainfall estimation algorithm is examined based on an extensive dataset of volume scan reflectivity and rain gauge rainfall measurements from the WSR-88D site in Melbourne, Florida. Radar rainfall estimates are evaluated based on the following radar–rain gauge statistics: mean difference (bias), normalized root-mean-square difference, and correlation coefficient. The spatiotemporal scales of interest are hourly accumulations over 4 km × 4 km grids. First, the authors demonstrate the convergence properties of the algorithm's adaptive parameter estimation procedure and conduct sensitivity tests of the system with respect to changes in the parameter values. Second, the major components of the algorithm are compared with the operational WSR-88D Precipitation Processing Subsystem. The authors show reduction in the radar–rain gauge root-mean-square difference up to 40%, resulting from the new parameterization schemes and the real-time calibration procedure. When rainfall classification is included, the reduction is higher (up to 50%). The authors show that correction for rain field advection moderately improves estimation accuracy (up to 20%). Finally, the authors show that the algorithm can effectively remove range-dependent systematic errors in radar observations.

1. Introduction

A multicomponent algorithm for real-time rainfall estimation based on radar reflectivity and in situ rain gauge rainfall measurements was presented by Anagnostou and Krajewski (1999). The algorithm produces hourly rain accumulations at the Hydrologic Rainfall Analysis Products (HRAP) grid (about 4 km × 4 km). The system includes vertical reflectivity integration, reflectivity to rainfall-rate transformation (Z–R), and range-effect correction. The algorithm also uses rainfall classification, beam–height-effect correction, and advection correction; its parameters are adjusted in real time.

To test the algorithm, we designed and conducted numerical experiments using radar and rain gauge data. The radar observations are from the Melbourne, Florida, WSR-88D (KMLB). The rain gauge data consist of observations from three networks: the South Florida Water Management District; the Kennedy Flight Center network located in Cape Canaveral, Florida; and the St. John's, Florida, network. The observations span the period of two months: 3 August–30 September 1995. During this period, Hurricane Erin and Tropical Storm Jerry passed over the area.

The algorithm-generated rain products are compared against the operational WSR-88D Precipitation Processing Subsystem (PPS) estimates (Fulton et al. 1998). These comparisons are used to demonstrate relative improvements coming from the various components of the algorithm with respect to the operational PPS. Improvement is quantified in terms of the reduction of 1) the radar–rain gauge root-mean-square (rms) differences and 2) the long-term, range-dependent radar rainfall bias. The algorithm is also compared with the PPS operated with optimal parameters. The PPS calibration is discussed in Anagnostou and Krajewski (1998). The comparison is based on an independent set (i.e., it is not included in the calibration) of rain gauge data. In addition, we examine the convergence properties of the algorithm's calibration procedure and assess the sensitivity of the system with respect to changes in the parameter values.

We also investigate the significance of rainfall classification for rainfall estimation. The hypothesis to be tested is whether the distinction between convective and stratiform cloud based solely on storm morphology, as inferred from volumetric reflectivity data, leads to changes in Z–R and range-effect correction parameters. Finally, we tested the algorithm's advection correction scheme by quantifying the resulting benefits.

The paper is divided into the following sections. Description of the data used in this study is provided in section 2. Evaluation of the algorithm's real-time pa-

* Current affiliation: Department of Civil and Environmental Engineering, University of Connecticut, Storrs, Connecticut.

Corresponding author address: Dr. Emmanouil N. Anagnostou, University of Connecticut, 261 Glenbrook Road, U-37, Storrs, CT 06269.
E-mail: manos@agnes.gsfc.nasa.gov

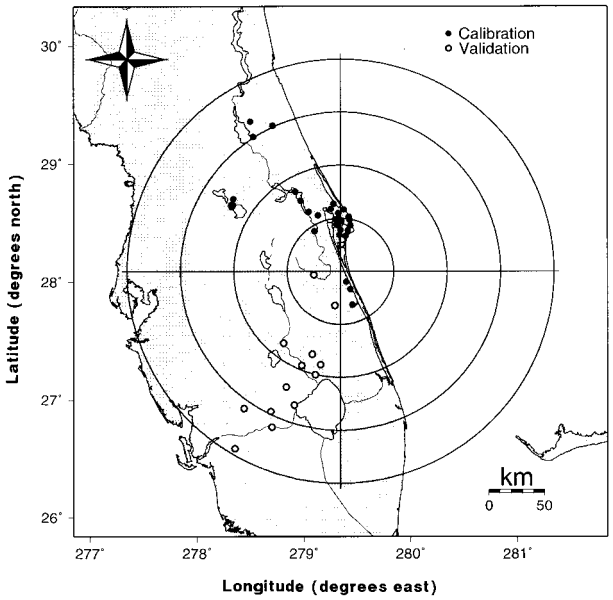

FIG. 1. Florida map with the KMLB WSR-88D radar and rain gauge locations. The circles correspond to 50-km ranges.

rameter estimation framework is presented in section 3, while a sensitivity analysis of the algorithm's main parameters is presented in section 4. An analysis of the algorithm's performance and the significance of its various components in the context of WSR-88D rainfall estimation accuracy is offered in section 5. Conclusions and proposals for future research investigations are offered in section 6.

2. Data

The dataset used in this study consists of two months of volume scan reflectivity observations from the Melbourne WSR-88D site. Rainfall measurements from 46 rain gauges, located within a 200-km radius from the radar, are used. This dataset is part of an ongoing effort by the National Aeronautics and Space Administration's (NASA) Tropical Rainfall Measuring Mission (TRMM) project in support of validation of space-based rainfall products. Details on the data statistics and quality can be found in Krajewski et al. (1996).

The radar location and the positions of the rain gauges are shown in Fig. 1. The rain gauge network is divided into two clusters. The first cluster, which is used for calibration of the algorithm, has 33 rain gauges and covers the upper-left radar sector. The second cluster, which is used for validation, has 13 rain gauges and covers the lower-left radar sector. The separation distance between the clusters makes the clusters spatially independent at the scale of hourly rainfall accumulation.

To overcome the high demands for computer storage required to process the two months of WSR-88D reflectivity data, a compression scheme was used to reduce the data size. First, the compression scheme of Kruger and Krajewki (1997) is applied to the raw (Crum et al. 1993) volume scan reflectivity data. This results in about a 10:1 compression ratio. Next, data files containing the raw reflectivity data that correspond to the HRAP pixels, which include rain gauges, are created. These files, hereafter referred to as ''small files,'' are coded and transformed from ASCII to binary code to further reduce their size. Subsequently, the system is modified to read the raw reflectivity data from the small files and to evaluate the objective function [Eq. (11) in Anagnostou and Krajewski (1999)], during the period of interest. This two-level compression technique can reduce the data storage by several orders of magnitude, depending on the radar–rain gauge data sample size.

3. Evaluation of the parameter estimation procedure

An important element that distinguishes this algorithm from others is its real-time parameter estimation scheme, which is based on a stochastic adaptive optimization method. The purpose of this section is to assess the efficiency of this scheme. The parameters to be optimized and their initial values are shown in columns 1 and 2, respectively, of Table 1. The efficiency of the parameter estimation procedure is evaluated based on 1) the convergence characteristics of the optimized parameters and 2) comparisons of the converged parameters with optimal parameter values derived from an offline global optimization method. The parameters of the algorithm's mean-field bias model component are not evaluated in this study. The bias model was examined in a data-based intercomparison study by An-

TABLE 1. The system's default and optimal parameter values.

Parameter	Description	Default	Optimal
S_x	Slope of range correction	10	45
$Z_{\min}$	Lower reflectivity threshold	0	5
$Z_{\max}$	Upper reflectivity threshold	50	52
A	Z–R relationship multiplier	200	230
B	Z–R relationship exponent	1.3	1.64
b_c	Ratio of convective/stratiform Z–R multipliers	1.0	1.24
A_{rc}	Convective range correction	0.0	−0.4
A_{rs}	Stratiform range correction multiplier	0.0	−0.5

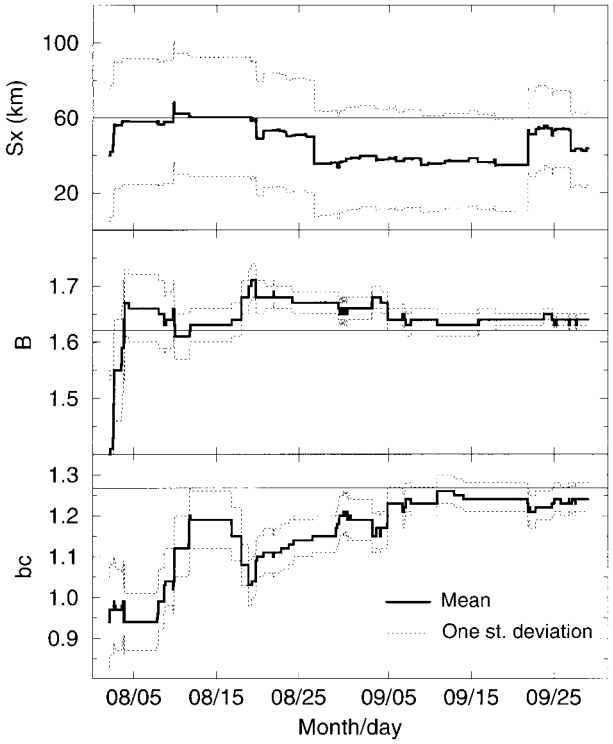

FIG. 2. Traces of S_x (upper panel), B (middle panel), and b_c (lower panel) parameter values.

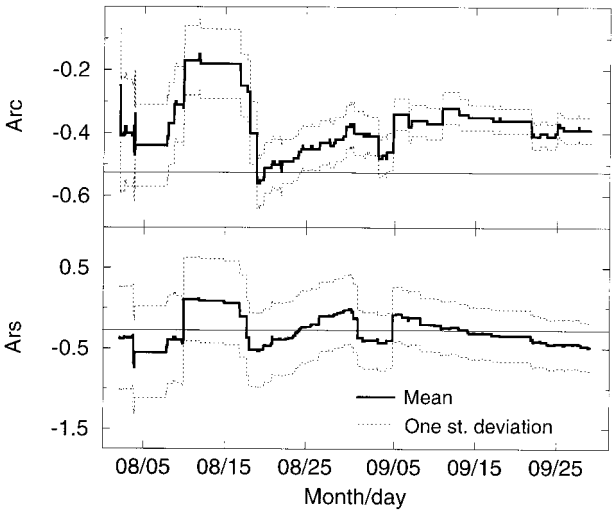

FIG. 3. Traces of A_{rc} (upper panel) and A_{rs} (lower panel) parameter values.

agnostou et al. (1998), in which the bias model appeared to perform better than the other models.

Figures 2 and 3 show the traces of the algorithm parameter values. The time step is 1 h, and the data period is 3 August–30 September 1995 (59 days). The thick solid lines represent the parameters' mean values, and the dashed lines are their one standard deviation upper and lower bounds. We note that during the parameter estimation none of the parameters were constrained by upper or lower bounds. In spite of this, the parameters do not take on, or converge to, physically unrealistic values at any time during the optimization. The parameter values were normalized with respect to their corresponding default values. This was done so that all parameter values, which are optimized, are in the same order of magnitude. A similar approach was followed by Kitanidis and Bras (1979) in an effort to calibrate a hydrologic model.

All figures show that as time progresses the fluctuations of the estimated parameter values and their uncertainty bounds decrease, which is an indication of convergence. It is interesting to note that even after two months of online calibration there are still fluctuations in the final parameter values. The parameter estimation scheme is designed to capture large temporal (e.g., month, season) and geographic variations of the algorithm's parameter values. Small timescale variations in the parameter values due to abrupt changes in the storms' microphysical processes are smoothed out by this method. The erratic behavior in the beginning of the parameter estimation is mainly due to data sampling uncertainty rather than actual parameter fluctuations. The radar–rain gauge rms sensitivity results, which are presented in the next section, indicate a minimal amplitude of these fluctuations when the sensitivity of the algorithm compared to parameter changes is low. It is most likely that these fluctuations are due to the sampling uncertainties in radar–rain gauge difference statistics resulting from 1) the huge difference in the two sensors' spatial sampling areas (eight orders of magnitude) and 2) the extreme small-scale rainfall variability (Ciach and Krajewski 1999; Anagnostou et al. 1998).

Finally, notice that the parameter values adjusted in real time converge to values estimated from an offline global optimization procedure (Anagnostou and Krajewski 1998). The procedure identifies the parameter values that minimize the radar–rain gauge rms difference [Eq. (11) of Anagnostou and Krajewski (1999)], evaluated as the final rainfall products over the whole data period (59 days). The offline optimization parameter values are plotted in Figs. 2 and 3 using straight solid lines. It is apparent that the offline optimization parameter values are close to the one standard deviation bounds of the adaptively estimated parameters. It is expected, in cases of larger data samples and rainfall regimes with smaller variability, that the agreement would be even better. The final parameter values derived in real time are shown in column 3 of Table 1. Notice that all of the parameters converge to values different from the default values.

4. Sensitivity analysis

In the previous section, we presented the optimal parameter values estimated based on the real-time cali-

TABLE 2. Conditional (rain gauge rainfall > 0.3 mm h^{-1}) data sample statistics.

Rain gauge network	Calibration	Validation
Hours of rain	410	301
Number of radar–gauge pairs	2380	1040
Rain accumulation (mm per gauge)	376	323
Quantiles (10% and 90%) (mm h^{-1})	(0.5, 11)	(0.5, 12)

bration procedure. In this section, we discuss the significance of these parameters in terms of the overall performance of the algorithm. We systematically explore the algorithm's multiparameter space in the vicinity of the optimal solution. We evaluate the sensitivity of the rms criterion with respect to changes in the values of one or, simultaneously, two parameters of the algorithm; the other parameters are kept at their optimal values. The rms is computed conditionally on the hourly rain gauge rainfall (i.e., only radar–rain gauge pairs, where rain gauge hourly rainfall is greater than 0.3 mm are included) and is normalized by the corresponding conditional mean hourly rain gauge rainfall. Table 2 presents conditional (rain gauge rainfall greater than 0.3 mm h^{-1}) data sample statistics.

The first investigated parameter is the hybrid reflectivity scan construction parameter, S_x. This parameter specifies the maximum range up to which vertical integration is applied. Figure 4 (left panel), where rms (%) is plotted against S_x values, shows that the optimal S_x value is in the range of 50–70 km. These results indicate a mean height of the integrated layer of about 2 km.

The next investigated parameter is the exponent B of the nonlinear Z–R relationship [Eq. (3) in Anagnostou and Krajewski (1999)]. Parameter A of the Z–R relationship is not optimized, but its value is adjusted by removing the hourly mean-field radar–rain gauge multiplicative bias [Eq. (5) in Anagnostou and Krajewski (1999)]. Figure 4 (right panel) shows the effect of parameter B on rms. There is a distinct minimum in rms for B values between 1.6 and 1.7. The rms gradient is weak close to the minimum, and at B values greater than the minimum, but it is strong for B values in the range between 1.1 and 1.5.

The maximum reflectivity threshold is the algorithm's parameter we discuss next. This upper-reflectivity threshold provides a quick and inexpensive control of hail effect, which is mostly responsible for the erroneously high values (i.e., greater than 50 dBZ) in the reflectivity data. Figure 5 shows the contours of rms versus B and $Z_{\max}$ parameter values. The contours of Fig. 5 indicate that there is no distinct minimum but a line of minima along the diagonal. The collinearity between B and $Z_{\max}$ values, shown in the figure, indicates dependence between the two parameters. This dependence can be explained by the Z–R relationship: when B increases, the maximum reflectivity threshold should increase accordingly to maintain the optimum maximum

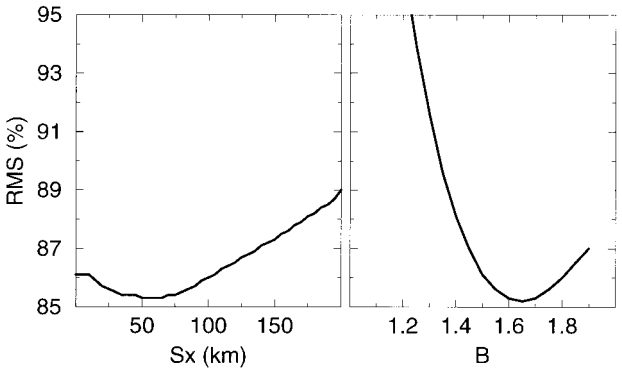

FIG. 4. Relative rms difference vs S_x (left panel) and B (right panel).

rainfall rate. Nonexistence of a distinct minimum in the B–$Z_{\max}$ space is explained either as lack of significant hail effect in the radar–rain gauge dataset used or as a weakness of the single threshold method to distinguish hail from rain returns.

The final element of this sensitivity study is devoted to the algorithm's rain regime classification-based parameters. A main difficulty of this case is the small contribution (about 8%) from stratiform precipitation to the overall precipitation volume (see column 4 of Table 3). To moderate this problem, the sensitivity runs were made only for the days during which the contribution from stratiform precipitation was higher than 10%. The first investigated parameter is the convective–stratiform ratio (b_c) of the Z–R multiplier. This ratio differentiates the convective and stratiform multiplicative coefficient of the Z–R relationship. Figure 6 shows the rms sensitivity with respect to changes in b_c. Notice that there

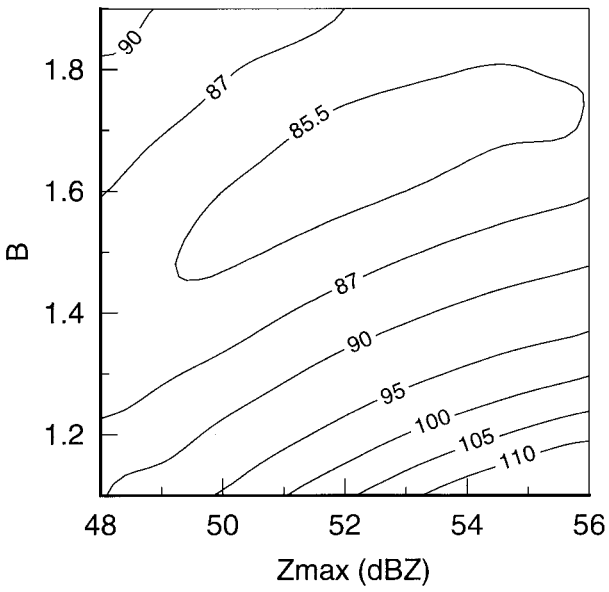

FIG. 5. Relative rms difference vs $Z_{\max}$ and B parameters.

TABLE 3. Radar–rain gauge comparison statistics for each day with a sample size greater than 20 pairs. Total rainfall accumulation is 3524 mm. Parameter CV is the ratio of standard deviation to mean rain gauge rainfall; C/S is the fraction of convective rain to the total rain; CC is the radar–gauge correlation, defined by Eq. (3); and the rest of the parameters are defined in the text.

Date	Accumulation (mm)	CV	C/S (%)	Bias	rms (%)	CC
3 Aug	131	0.99	87.5	1.05	64	0.76
4 Aug	54	0.78	88.0	0.67	87	0.86
9 Aug	75	0.99	93.2	0.75	77	0.80
10 Aug	162	1.56	90.0	1.18	81	0.87
20 Aug	102	1.24	95.0	0.80	110	0.70
21 Aug	118	1.43	93.9	1.03	97	0.74
22 Aug	66	1.07	94.4	0.92	46	0.91
23 Aug	238	1.07	90.2	1.25	77	0.72
24 Aug	471	1.32	86.0	1.54	62	0.93
25 Aug	525	1.23	89.9	1.23	84	0.77
30 Aug	120	1.21	90.6	1.47	63	0.91
31 Aug	196	1.05	94.5	1.01	64	0.83
1 Sep	77	1.66	76.7	1.38	100	0.94
2 Sep	149	1.15	91.3	0.96	74	0.79
5 Sep	164	1.00	92.9	1.02	47	0.88
6 Sep	81	1.03	92.2	0.65	108	0.73
7 Sep	127	1.40	85.4	1.09	121	0.52
8 Sep	126	0.93	95.7	0.94	46	0.88
9 Sep	39	1.63	83.9	0.64	94	0.89
10 Sep	124	1.33	94.9	0.88	64	0.89
12 Sep	104	1.29	93.0	1.57	84	0.86
16 Sep	51	1.88	92.8	0.86	139	0.69
18 Sep	27	0.65	87.3	0.86	70	0.66
27 Sep	102	1.35	89.2	0.90	77	0.83
28 Sep	96	1.53	92.4	1.13	69	0.91
Average	141	1.23	90.4	1.03	80	0.81

is a flat line of minima between 1.1 and 1.4. The rms gradients are strong below 1.1, and they weakly increase as b_c values increase. The general observation is that the convective Z–R multiplier is from 1.1 to 1.5 times larger than the stratiform multiplier. This result is supported by Tokay and Short (1996), who studied a large number of drop size distribution data.

The last two classification-based parameters are the convective (A_{rc}) and stratiform (A_{rs}) coefficients of the algorithm's range correction formula. Figure 7 shows the rms versus parameters A_{rc} (left panel) and A_{rs} (right panel). Comparing the two panels, one can notice that rms is more sensitive to changes of the A_{rc} parameter. This is most probably due to the higher contribution to the overall rms from the convective rainfall rates relative to the stratiform rainfall rates. It is interesting to note the significant difference in the optimal values of the A_{rc} and A_{rs} parameters. The optimal A_{rc} is around -0.5, while the optimal A_{rs} is between 0.0 and 0.2. This is explained by the differences in the microphysical properties of convective and stratiform precipitating clouds (e.g., vertical velocity and hydrometeor size and phase distribution), which result from different reflectivity profiles.

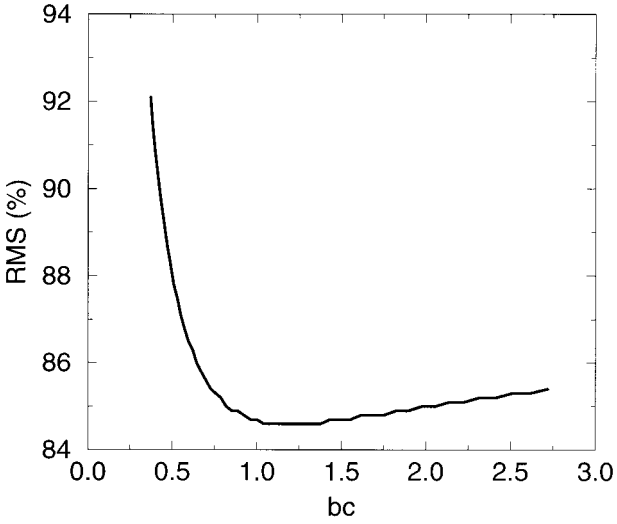

FIG. 6. Relative rms difference vs b_c parameter.

5. Rainfall estimation performance

a. Radar–rain gauge comparisons

The algorithm's performance is assessed by comparing its gridded hourly rainfall products with corresponding, independently obtained rain gauge rainfall reports. These rainfall reports come from the validation rain gauge network. The system's rainfall estimates are evaluated based on the following radar–rain gauge difference statistics: 1) mean bias, 2) relative rms (rms normalized by the mean rain gauge rainfall), and 3) correlation coefficient (CC). These statistics, computed for each day (conditionally to rain gauge rainfall rate greater than 0.3 mm h^{-1}), are as follows:

$$\text{bias}(d) = \frac{\langle R_g \rangle_d}{\langle A \rangle_d} \tag{1}$$

$$\text{rms}(d) = \langle (R_g - A)^2 \rangle_d \tag{2}$$

$$\text{CC}(d) = \frac{\langle R_g A \rangle_d - \langle R_g \rangle_d \langle A \rangle_d}{[(\langle R_g^2 \rangle_d - \langle R_g \rangle_d^2)(\langle A^2 \rangle_d - \langle A \rangle_d^2)]^{1/2}}, \tag{3}$$

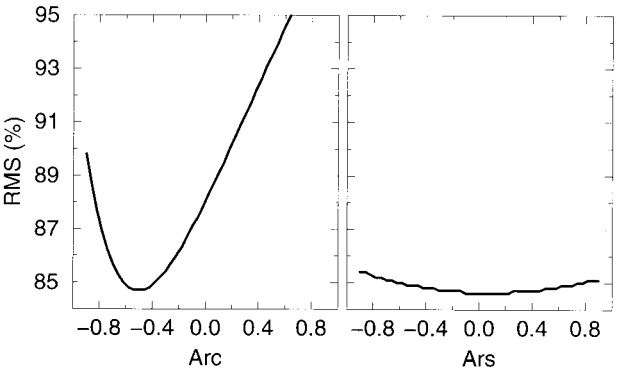

FIG. 7. Relative rms vs A_{rc} (left panel) and A_{rs} (right panel).

where $\langle V \rangle_d$ of variable V (V: R_g, A, R_gA, R_g^2, A^2, $R_g - A$) is defined as

$$\langle V \rangle_d = \sum_{s=1}^{N_s(d)} \sum_{j=1}^{N_g} [V(s, j) | R_g(s, j) > 0.3], \qquad (4)$$

where d, s, and j are day, hour, and radar–gauge pair indices; $N_s(d)$ and N_g are the number of rainy hours and radar–gauge pairs of day d; R_g is the rain gauge rainfall (mm h^{-1}); and A is the radar-estimated rainfall (mm h^{-1}). The conditioning on the radar–rain gauge difference statistics is performed to avoid problems related to the high zero intermittence of hourly precipitation and to evaluate the algorithms only for significant precipitation events that are of concern in real-time operation.

Table 3 summarizes the results. Columns 2–4 show the mean hourly rainfall, coefficient of variation (CV = standard deviation/mean), and percent convective coverage, respectively. Columns 5–7 include the radar–rain gauge statistics (bias, rms, CC). Days with small sample sizes (less than 20 pairs) are not reported. This is done to minimize the sampling effect in the presented statistics. Column 5 shows that the mean daily radar–rain gauge differences are less than half of the mean daily rainfall. The correlation coefficient varies between 0.55 and 0.95, while the relative rms is between 45% and 140%. Both CC and rms seem to be sensitive to the variability of rainfall in the area. The rms (CC) tends to be higher (lower) for days when the CV of hourly rain gauge rainfall is high and vice versa. Overall, the hourly rms is less than the mean hourly rainfall; the systematic error is insignificant (bias = 1.03); and the CC is relatively high (0.81).

b. Comparison with the PPS

The algorithm's performance is now evaluated against the operational PPS. The significance of the new procedures is assessed in terms of the degree of improvement of rainfall estimation accuracy with respect to the PPS. The procedures are divided into the following three algorithms. The first algorithm (NC) includes the new procedures for vertical integration, Z–R transformation, range-effect correction, and the real-time calibration scheme. The second algorithm (YC) includes the above procedures and applies rain classification–based separation of the Z–R and range-effect correction parameter values. The third algorithm (AC) applies advection correction at the scan-to-scan rainfall products of the second algorithm. In the analysis presented herein, the three algorithms are examined against the PPS operated with optimal parameters (OP). The procedure used to calibrate the PPS is described in Anagnostou and Krajewski (1998).

The improvement criteria are 1) relative reduction of the rms difference and 2) reduction of the long-term range-dependent bias with respect to the operational PPS. The relative rms reduction (rrms) is defined as

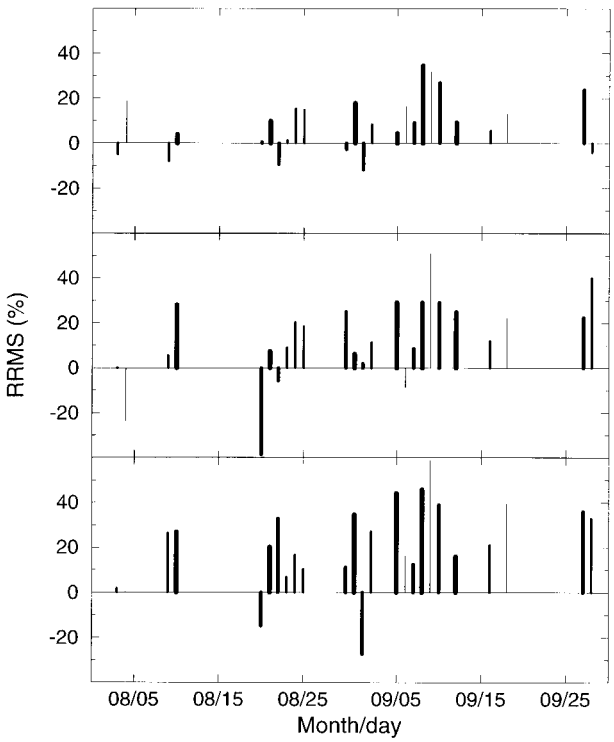

FIG. 8. Day-by-day-based relative rms reduction with respect to the operational PPS for the OP (upper panel), NC (middle panel), and YC (lower panel) algorithms. The bars' thickness is modulated by the class of daily rain gauge rainfall accumulation (0–100, 100–200, and >200 mm).

$$\text{rrms} = 100 \times \frac{\text{rms}_{\text{PPS}} - \text{rms}_{\text{ALG}}}{\text{rms}_{\text{ALG–PPS}}}, \qquad (5)$$

where rrms (%) is the relative rms reduction. Here rms_{PPS} is the radar–rain gauge rms difference of the operational PPS, while rms_{ALG} is the rms difference of algorithm ALG–ALG that symbolizes the various algorithms NC, YC, AC, and OP. For reasons discussed in section 5a, rms is computed conditionally to the rain gauge hourly rainfall ($R_g > 0.3$ mm h^{-1}). In the following, the algorithms' performance is synthesized on a day-by-day basis.

Figure 8 shows the rms reduction with respect to the operational PPS for the first two algorithms and the optimal PPS. It is apparent that both algorithms (NC and YC) are more effective than OP in reducing the rms. With classification included, the algorithm can reduce rms up to 50%. Comparing column 2 of Table 3 and Fig. 8, one can notice that in most of the days with significant mean rainfall intensity (greater than 5 mm h^{-1}) the rms reduction exceeds 20%. Also, in most of the days, classification appears to improve rainfall estimation accuracy. The relative improvement due to classification for each day is shown in Fig. 9.

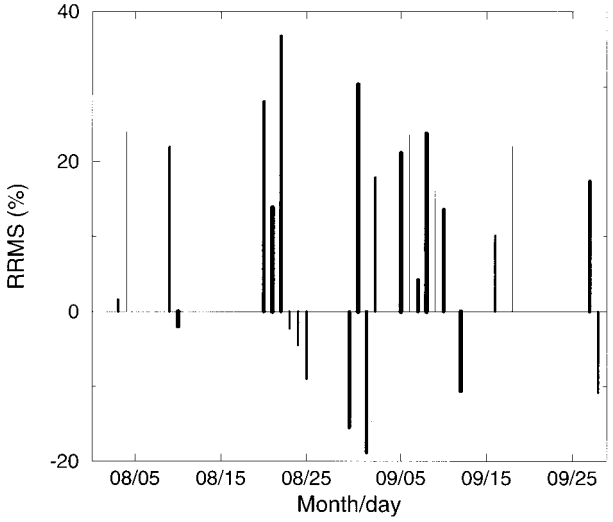

FIG. 9. Day-by-day-based relative rms reduction with respect to the NC algorithm for the YC algorithm. The bars' thickness is modulated by the class of daily rain gauge rainfall accumulation (0–100, 100–200, and >200 mm).

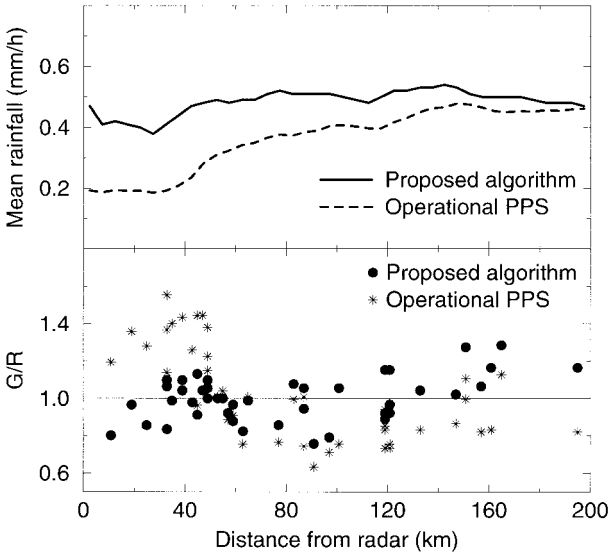

FIG. 11. Mean rainfall (upper panel) and rain gauge–radar mean rainfall ratio (lower panel) vs distance from the radar.

Figure 10 shows the relative rms reduction when advection correction is applied. Figure 10 is based on all (calibration and validation networks) radar–rain gauge pairs. One can see that overall advection correction reduces the radar–rain gauge rms difference. With the exception of one day, the rms increase due to advection correction does not exceed 5%. It should be noted that on the days during which the rms increase is close to 5%, the mean rainfall is low. On the other hand, the rms reduction due to advection correction can be up to about 20%, and in most of the days is greater than 5%.

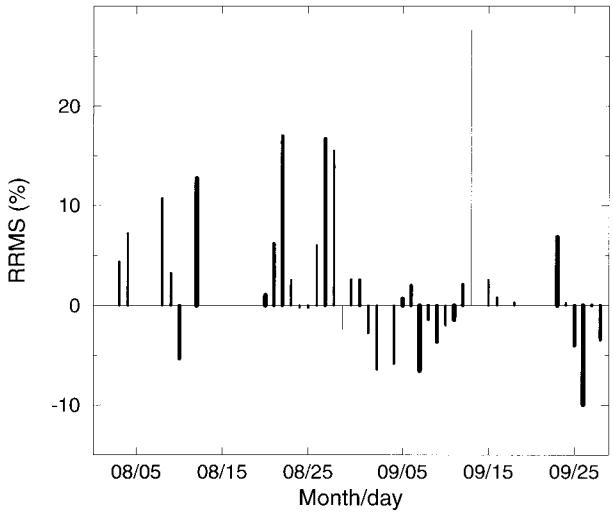

FIG. 10. Day-by-day-based relative rms reduction with respect to YC algorithm for the AC algorithm. The bars' thickness is modulated by the class of daily rain gauge rainfall accumulation (0–100, 100–200, and >200 mm).

This rms analysis demonstrates a moderate improvement due to advection correction.

The efficiency of the system's range-effect correction is demonstrated in Fig. 11. The upper panel of Fig. 11 shows the overall (both months) mean radar rainfall versus distance from the radar. Solid and dashed lines correspond to the new algorithm, including classification and the operational PPS, respectively. The lower panel of Fig. 11 shows the ratio between rain gauge and radar mean rainfall (G/R) over the rain gauge locations. Solid circles and asterisks correspond to the new algorithm and the PPS, respectively. In the first panel, note that the algorithm's rainfall estimates, in contrast to those from the PPS, have negligible range dependence. In the second panel, which evaluates the range dependence based on comparisons with rain gauges, unbiased estimates up to 150-km radar range are shown. At far ranges (greater than 150 km), though, there is an indication of approximately 20% overestimation. We speculate that this is an effect of the inadequate representation of these ranges in our calibration dataset.

6. Closing remarks

We present an evaluation of the real-time radar rainfall estimation algorithm formulated by Anagnostou and Krajewski (1999). An extensive dataset of radar and rain gauge observations from the Melbourne WSR-88D site was used for this purpose. Several issues were investigated, including 1) the convergence properties of the system's adaptive calibration procedure, 2) the sensitivity of the system with respect to parameter diversions from the optimal values, and 3) the significance of the different algorithm components in the context of WSR-88D rainfall estimation accuracy.

For the investigated dataset, we demonstrated an overall reduction of about 20% of the rms radar–rain gauge difference with respect to the operational PPS. We emphasized that discrepancies in comparisons between radar and rain gauge rainfall accumulations are due to 1) errors in radar-rainfall estimation and 2) sampling differences between point rain gauge rainfall and radar product grid area rainfall (4–16 km^2). For hourly rainfall accumulations, this area-point difference may be of similar magnitude to the corresponding rainfall estimation error, depending on the variability of rainfall in the area (Ciach and Krajewski 1999; Anagnostou et al. 1998). Considering also that the area-point difference does not depend on radar rainfall estimation procedures, one can understand that the rms reductions shown in this study represent only part of the actual reductions that occurred in the radar-rainfall estimation error. To be able to quantitatively demonstrate improvements in radar-rainfall estimation, the area-point difference should be determined and subtracted from the radar–rain gauge differences. Although statistical frameworks have been recently developed for this purpose (Ciach and Krajewski 1999; Anagnostou et al. 1998), we still lack systematic rainfall observations at subradar product grid scales to support such a task.

The adaptive parameter estimation component of the algorithm is a new procedure introduced in this research. We demonstrated that the procedure needs only a few rainy days to converge to the optimal parameter values of the algorithm. This makes our procedure attractive to new radar installations for which no prior information exists for adjusting the algorithm's parameters. Another advantage of our scheme is its potential to determine changes in the algorithm optimal parameter values related to storm-to-storm and seasonal variations of precipitation. However, as this study was limited by a single-season dataset, we could illustrate only storm-based parameter adjustments.

The potential for improvement of rainfall estimation from advection correction was not fully demonstrated in this study. This is due to the particularity of the summer season precipitation systems in Florida. It was a frequent occurrence that isolated convective cells developed within a small area, creating the false impression that there was a storm advection. In these situations the advection correction procedure, which is based solely on the morphology of the storm, provided erroneous estimates of the storm velocity. Better results are expected by applying this method to a different radar site associated with more organized precipitation systems (i.e., squall lines).

We believe that an important requirement that should drive radar-rainfall validation studies is the data sample size. In this research, we used two months of continuous radar and rain gauge observations. We are currently working toward compiling one year of radar data from the Tulsa, Oklahoma, WSR-88D. It is important to note that such extensive data-based studies require specialized data management and compression techniques.

Acknowledgments. We acknowledge and appreciate useful discussions with Dr. James A. Smith from Princeton University and Dr. Dong-Jun Seo from the Office of Hydrology of the National Weather Service. We also thank Tim O'Bannon, Operational Support Facility of the National Weather Service, and the two anonymous reviewers for their helpful comments on the original manuscript. This study was supported by the National Weather Service, under a cooperative agreement between the Office of Hydrology of the National Weather Service and the Iowa Institute of Hydraulic Research. It was also supported by NASA under Grant NAG-5-2094.

REFERENCES

Anagnostou, E. N., and W. F. Krajewski, 1998: Calibration of the WSR-88D Precipitation Processing Subsystem. *Wea. Forecasting,* **13,** 396–406.

——, and ——, 1999: Real-time radar rainfall estimation Part I: Algorithm formulation. *J. Atmos. Oceanic Technol.,* **16,** 189–197.

——, ——, D.-J. Seo, and E. R. Johnson, 1998: Mean-field radar rainfall bias studies for WSR-88D. *ASCE J. Hydrol. Eng.,* **3,** 149–159.

——, ——, and J. Smith, 1999: Uncertainty quantification of mean-areal radar rainfall estimates. *J. Atmos. Oceanic Technol.,* **16,** 206–215.

Ciach, G. J., and W. F. Krajewski, 1999: On the estimation of radar rainfall error variance. *Adv. Water Resour.,* in press.

Crum, T. D., R. L. Alberty, and D. W. Burgess, 1993: Recording, archiving, and using WSR-88D data. *Bull. Amer. Meteor. Soc.,* **74,** 645–653.

Fulton, R. A., J. P. Breidenbach, D.-J. Seo, D. A. Miller, and T. O'Bannon, 1998: The WSR-88D rainfall algorithm. *Wea. Forecasting,* **13,** 377–395.

Kitanidis, P. K., and R. L. Bras, 1979: Error identification in conceptual hydrologic models. *Applications of Kalman Filter to Hydrology, Hydraulics and Water Resources,* C. L. Chin, Ed., Department of Civil Engineering, University of Pittsburgh, 325.

Krajewski, W. F., and Coauthors, 1996: Radar-rainfall estimation studies for TRMM ground validation. IIHR Tech. Rep. No. 379, Iowa Institute of Hydraulic Research, University of Iowa, Iowa City, IA, 205 pp. [Available from Iowa Institute of Hydraulic Research, University of Iowa, Iowa City, IA 52242.]

Kruger, A., and W. F. Krajewski, 1997: Efficient storage of weather radar data. *Software Practice and Experience,* **27,** 623–635.

Tokay, A., and D. A. Short, 1996: Evidence from tropical raindrop spectra of the origin of rain from stratiform versus convective clouds. *J. Appl. Meteor.,* **35,** 355–371.